Commun Nonlinear Sci Numer Simulat 97 (2021) 105770

Contents lists available at ScienceDirect

Commun Nonlinear Sci Numer Simulat

journal homepage: www.elsevier.com/locate/cnsns

Research paper

Particle-based numerical modeling of a thin granular layer subjected to oscillating flow

B. Crespin [a,b], M.G. Clerc [c], G. Jara-Schulz [c,*], M. Kowalczyk [d]

[a] Université de Limoges, XLIM/ASALI, UMR CNRS 7252, Limoges F-87000, France
[b] Center for Mathematical Modeling, UMI (2807) UCHILE-CNRS, Santiago, Chile
[c] Departamento de Física and Millennium Institute for Research in Optics, Facultad de Ciencias Físicas y Matemáticas, Universidad de Chile, Casilla Santiago, 487-3, Chile
[d] Departamento de Ingeniería Matemática and CMM, Universidad de Chile, Casilla Santiago, 170-3, Chile

ARTICLE INFO

Article history:
Received 11 September 2020
Revised 11 January 2021
Accepted 14 February 2021
Available online 16 February 2021

Keywords:
Granular systems
Self-organizations
Numerical simulations

ABSTRACT

Self-organization is observed in granular systems under permanent energy injection. Various aspects of this phenomena have been characterized in experimental studies, however, due to the partial access to the evolution of granular media, numerous details of this self-organization process are unknown. Here, we investigate a simple, particle-based model that captures the dynamics of a quasi-two-dimensional shallow granular layer subjected to an air flow oscillating in time. Based on the numerical simulations, we characterize the phase diagram, structure and dynamics of domain walls, attractive standing waves, and reveal the origin of their wavelength. Our findings present a quite fair qualitative agreement with experimental observations.

1. Introduction

The granular matter is made up of a large number of small, solid components that are big enough to neglect thermal fluctuations, and which can flow like a liquid or remain still like a solid [1–5]. The dynamics of these media are mainly governed by solid contacts, that is, friction and collisions. Common examples are sand, seeds, nuts, powders, pills, gravel and avalanches, to name a few [1–5]. Due to the properties shared with fluids and solids, granular media are characterized by an intermediate behavior of matter between solid and liquid. In the last decades, much effort has been devoted to the study of the phenomena exhibited by granular matter. However, the richness and complexity of its static and dynamical properties still present a major challenge in physics and engineering science. The fluidized granular matter has attracted the interest of the scientific community for its interesting and unexpected dynamics [1–5]. Due to the dissipative nature of granular matter, to fluidize such a system external energy must be supplied, for example by mechanical agitation or an up-flow of gas strong enough to counter gravity. This last mechanism of fluidization is used in the industry for mixing solid particles with liquids or gases [6]. Indeed, it is of prominent technological importance in catalysis of gas-sphere reactors, transport of powders, and combustion of powders to mention a few [6]. From the point of view of the formation of the dissipative structure [7–10], fluidized granular media subjected to an oscillating flow have been shown to exhibit patterns, domain walls, convections, and localized structures, among others (see the textbook [5] and reference therein).

* Corresponding author.
E-mail address: gladys.jara-schulz@c2n.upsaclay.fr (G. Jara-Schulz).

https://doi.org/10.1016/j.cnsns.2021.105770
1007-5704/

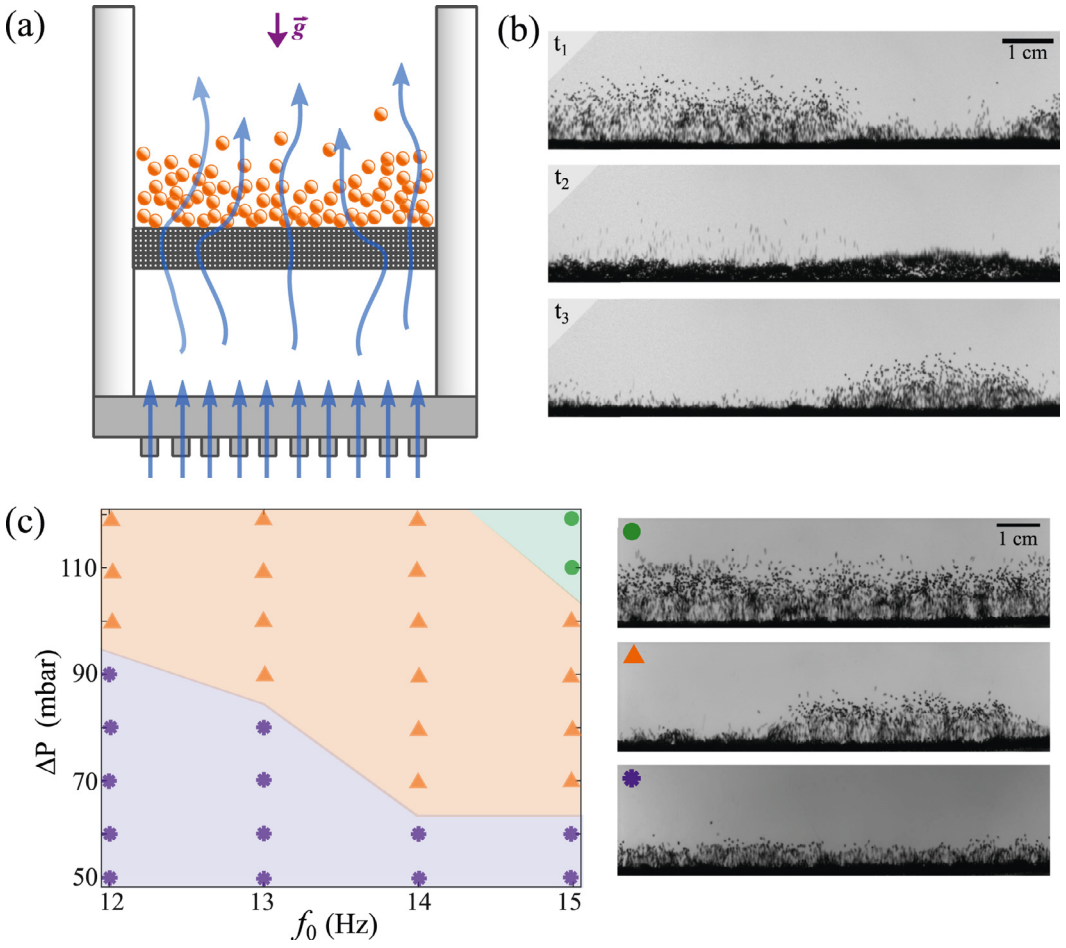

Fig. 1. A quasi-two-dimensional shallow granular layer subjected to an airflow oscillating in time with zero reference pressure $P_0 = 0$. (a) Schematic diagram of the experimental Hele-Shaw cell consisting of granular layers set on a porous bottom subjected to a temporarily modulated airflow. (b) Temporal snapshots for a granular domains (kinks) $t_1 < t_2 < t_3$. (c) Experimental phase diagram for the air pressure (ΔP) versus the modulation frequency (f_0) of the air flow. The symbols represent: (•) the noise patterns regime (precursors), (▲) the kink regime, and (∗) the homogenous fluidized regime.

Self-organization can be studied through the use of a Hele-Shaw cell with time-periodic airflow for a quasi-two-dimensional granular bed deposited on a porous surface [11]. Fig. 1a shows a schematic representation of this setup and the typical self-organization patterns observed. For large enough flows, the interaction between the flow, gravity, and grains allows the granular medium to fluidize. That is, the particles of the granular medium are brought to permanent, random motion. By further increasing the intensity of the flow, the fluidized granular bed can exhibit patterns, domain walls, and complex spatiotemporal dynamics [11–16], see Fig. 1. Similar dynamics are observed when considering a thin channel with a vertically excited granular medium [2,17–19] in which the energy is injected into the system through the collision of the grains with the walls of the container. Considering the non-inertial reference system fixed to the container, molecular dynamic simulations describe the vertically driven granular media. This type of strategy has been successful in understanding the internal dynamics of granular systems, which is difficult to access experimentally (see review [20] and references therein). Thanks to it was possible to understand the structure of convection rolls [21–25], Faraday waves [26], and phase separation [27]. On the contrary, the internal dynamics of fluid-driven granular media has not been completely understood because the existing studies are mainly experimental and give only partial information about the granular dynamics. One strategy to understand and model these physical systems has been to consider particles as hard spheres immersed in a fluid, which is governed by the fluid equations (Navier-Stokes) [28–30]. This allows to explain segregation [28], convection and fluidization [29], and the formation of sand ripples [30]. The drawback of this approach is its complexity and high demand for computational capacity, which limits the number of constituents of the granular medium. This work aims to present a simple, numerical model that captures the dynamics of a quasi-two-dimensional shallow granular layer subjected to an airflow oscillating in time. Based on particle-based numerical simulations, we characterize the phase diagram, structure and dynamics of domain walls (granular kinks), attractive standing waves (Faraday waves), and reveal the origin of their wavelength. The numerical findings exhibits an excellent qualitative agreement with the experimental observations.

2. Dissipative structures in a shallow granular layer subjected to an airflow oscillating in time

A quasi-two-dimensional shallow granular layer subjected to an airflow oscillating in time experimental setup consists of a Hele-Shaw cell, depicted in Fig. 1(a), made up of two glass plates 250 mm wide, 320 mm high, and separated in parallel by a distance of 3.5 mm. A set of metal meshes placed between the plates serves as a porous bottom on which monodisperse bronze spheres (diameter d = 350 m) are deposited, forming a thin granular layer the dimensions of which are 5d high, 400d long, and 10d deep. The entire structure is mounted on an aluminum frame.

The granular layer is forced by periodic airflow (similar to the ones described in [11–16]), which comes from an air compressor and is regulated by an electromechanical valve. The valve opens and closes following a voltage signal sent from a function generator through a power amplifier. A harmonic sinusoidal signal is sent with a frequency f_0 and a non-zero offset. This generates a periodic pressure $P(t) = P_0 + \Delta P$ of the air, where P_0 is a non zero reference pressure and ΔP is the amplitude of the modulated pressure through a periodic function with period $1/f_0$ [14]. The control parameters in our experiments are f_0 and ΔP. For monitoring the spatiotemporal evolution of the granular layer and data acquisition, a CCD camera is placed in front of the cell about 15 cm away and perpendicular to the Hele-Shaw cell. Images captured by the camera have 780×200 px of size, with a conversion factor of 78 px/cm. The acquisition frequency was set at $f_0/2$. The cell is illuminated with white light from behind with an arrangement of led lights and a screen that diffuses the light, in order to enhance the contrast between the motion of the grains and the background.

In the regime of low pressure, initially static granular layer starts to fluidize at a critical pressure [11–16] and oscillates with the forcing frequency while remaining flat. Fig. 1c shows the phase diagram of this granular system, in which the violet region represents the zone of the fluidized granular layer. A typical snapshot of the fluidized layer is included in the bottom panel. As the pressure amplitude increases, the granular layer undergoes a destabilization through a parametric instability, which generates domain walls or granular kinks [15,16], see Fig. 1(b). This instability is of supercritical nature, that is, near the transition, the height difference between domains is decreasing continuously as the square root [11,15,16]. Domains are characterized by exhibiting disordered patterns. Different domains separated by walls can coexist. Fig. 1b shows a temporal sequence of two domains walls. The dynamics of the positions of the walls is characterized by random fluctuations and hopping dynamics of the interfaces. The orange region in Fig. 1(c) illustrates the area where granular kinks are observed. Notice that these granular domains are observed for lower pressure amplitudes if the modulation frequency of the air-fluid increases. Further increasing the pressure amplitude, the wall domains become unstable and give rise to granular patterns [16]. These patterns correspond to subharmonic standing waves, which are the granular equivalent of those observed by Faraday in a vertically driven water container [31]. The green region in Fig. 1(c) shows the regime of parameters where Faraday waves begin to be observed. These noisy patterns are usually referred to as precursors [32] and the top panel of Fig. 1(d) shows their typical representative. It is worth mentioning that in the case of small Hele-Shaw cells the domain walls are not observed [14] and the fluidized granular layer undergoes a spatial parametric transition, which originates the Faraday waves.

3. Particle-based numerical modeling

In the following, we describe our model that simulates the behavior of the quasi-two-dimensional shallow granular layer subjected to an airflow oscillating in time. Then we give a complete description of the different stages of the algorithm.

3.1. Numerical representation of a quasi-two-dimensional granular layer

Granular materials can be modeled with a large collection of discrete elements represented by spherical particles [20–22,26,27,33–35]. As mentioned before, models based on fluid equations and hard spheres, have been successful in explaining different phenomena [28–30]. However, their ability to reveal the mechanisms of emerging phenomena is limited, due to a large number of components. Other efficient implementations based on the discrete element method were proposed [36] and they are in fact similar to the molecular dynamics method used to study three-dimensional gravity-driven granular flow of sand in a container [20–22,26,27,37]. Inspired by this last point of view we build a two-dimensional model where each particle is described by a hard disc with constant mass and diameter, and varying physical quantities such as its position and velocity (cf. Fig. 2) [38]. For the sake of simplicity, we have not considered rotation; that is, we model the particles as rigid non-rotating solids. At each iteration of the simulation positions and velocities are updated using a fixed time step. Gravity is taken into account as a global external uniform force applied to all particles, which are constrained to stay inside a rectangular simulation box. The position of the particles is described by two cartesian coordinates, respectively x, the horizontal and y, the vertical component. There is no long-range force between the particles and when two particles collide a contact force is applied in order to conserve the linear momentum and account for the dissipation of the energy by using a constant restitution coefficient [20–22,26–30]. In addition, we also include a force to account for the shear friction between particles and simulate pile formation with a specific angle of repose.

The simulation box is divided in columns, each particle being assigned to a single column based on its horizontal position x, see Fig. 2. The average height in each column is used to compute the instantaneous height of the granular medium $h(x, t)$. Fig. 2 schematically illustrates the granular system and the algorithm used to evolve grains, where arrows attached to the disks representing the particles account for their respective speeds and directions of propagation. The vertical lines

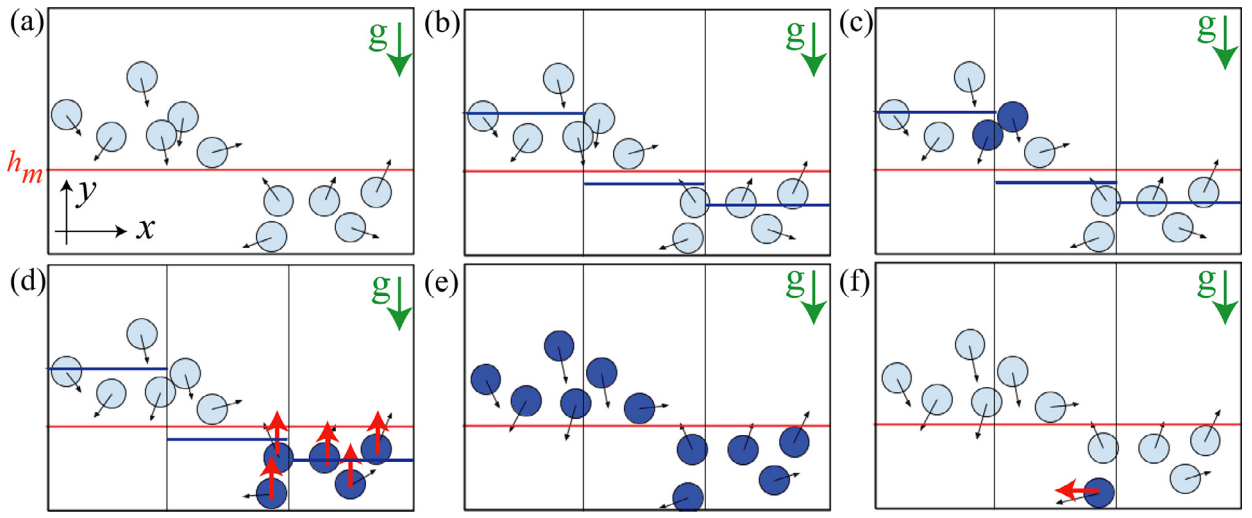

Fig. 2. Schematic representation of the algorithm computation loop. (a) Positions and velocities, where disks represents the grains and arrows their respective velocities. $\vec{g}$ and h_m stand, respectively, for the gravity field and the critical height at which the drag force is negligible compared to the weight. (b) Computation of the average height in each column depicted with a blue segment line. (c) Use of collision rule for particles in contact. (d) Application of an upwards drag force, formula (1), representing the injection of air. Red arrows account for particles under the influence of the drag force. (e) Update position and velocities. (f) Application of the horizontal force for particles in contact with the ground.

illustrate the limits of granular columns, and the blue horizontal line segments account for the average height. The effect of the oscillating airflow on particles is modeled by a drag force $\vec{f}(t)$ induced on the particles [4], which is effective if and only if the average height in a column is below a control parameter h_m. The drag force reads

$$\vec{f}(t) = \begin{cases} F\left(1 - \frac{y^3}{h_m^3}\right)\hat{y}, & y \leq h_m \text{ and } \sin(\omega t) \geq 0, \\ 0, & y \leq h_m \text{ and } \sin(\omega t) < 0, \\ 0, & y > h_m, \end{cases} \tag{1}$$

where F is a parameter representing the amount of air injected in the system, which we have denominated as pump force, and $T = 2\pi/\omega$ corresponds to the period where the airflow is applied.

As in the experiment, the upward force is applied only during a limited number of iterations, with an input parameter called N_A, where $T = N_A dt$ and dt accounts for the interaction time. We note N_F the total number of iterations for a complete cycle : when the number of iteration reaches N_F the whole process starts again.

Hence, ω is computed as the ratio of the number of pushing iterations N_A over the total number of iterations N_F. The parameter h_m accounts for the critical height at which the drag force is negligible compared to the weight. Hence, the drag force applied upwards is stronger for particles located near the ground, and quickly fades away until height h_m is reached.

Numerical simulations with different h_m qualitatively show the same type of observed dynamic behavior. Hence, we have concentrated on modifying the numerical parameters equivalent to those controlled in the experiment.

Recently, an interesting induced dynamics has been demonstrated when the granular bed granular layer assembly is tilted [11,39]. To account for any misalignment in mounting inclination, we include a constant external horizontal force $\vec{B} = B_0\hat{x}$. This force is applied when particles come in contact with the ground, and effectively mimics the way the particles slowly drift left or right depending on the inclination.

The main parameter of our algorithm is the threshold height h_m (red line in the figures below) used to determine which particles are pushed up and to simulate the injection of air.

3.2. Simulation algorithm and parameters

Our simulation is controlled by different parameters presented in the previous section. Constant parameters, such as the size of the vertical columns partitioning the simulation box, are fixed and tuned manually whereas variable parameters take values in a fixed range. Their complete list is reported in Table 1, except for the mass of a particle which set to 1 for the sake of simplicity.

The main stages of the simulation algorithm are described below :

(a) *Initialization:* each particle is given a random position and velocity obtained from a Gaussian distribution (Fig. 2a), and the iteration number i is set to 0.
(b) Assign each particle to the corresponding column, then compute the average height c_y in each column. Fig. 2b shows an example with 3 columns, where the average height is depicted as a blue horizontal line.

Table 1
Table of parameters.

Parameter	Notation	Constant value or range
number of particles	n	[1200, 5000]
time step	dt	0.035
gravity acceleration	g	0.1
critical height	h_m	60
vertical pump force	F	[0, 2.5]
horizontal force	B_0	[−0.1, 0.1]
num. of iterations for one cycle	N_F	[85, 95]
num. of pushing iterations	N_A	30
diameter	d	6
size of partition columns	S	8
spring coefficient	k	0.7
friction coefficient	f_c	0.995
restitution coefficient	e	[0, 1]

(c) *For each pair* (p_1, p_2) *of particles:* detect and handle possible overlaps using Algorithm 1, in order to simulate near-elastic collisions and pile formation (see Fig. 2c where two particles in contact are represented in dark blue).
(d) *For each particle:* if the iteration number $i \in [0, N_A]$ and the average height of the column assigned to this particle $c_y < h_m$, then compute the drag force $\vec{f}(t)$ for this particle using Eq. (1). Fig. 2(d) shows an example where only particles marked in dark blue are modified.
(e) *For each particle:* update velocity and positions using a simple first order scheme:

$$\begin{aligned} \vec{v}(t+dt) &= \vec{v}(t) + (\vec{f}(t) + g\hat{y})\ dt, \\ \vec{p}(t+dt) &= \vec{p}(t) + \vec{v}(t)\ dt, \end{aligned} \tag{2}$$

where g represents gravity. As shown in Fig. 2(e), all particles are modified during this step.
(f) *For each particle:* if the particle collides with the left, right or top walls, a simple elastic collision is applied. If it collides with the ground, the constant horizontal force $\vec{B} = B_0\hat{x}$ is applied towards the left or right to implicitly represent the inclination of the simulation box, as shown on Fig. 2f for one particle marked in dark blue.
(g) go back to the beginning of the computation loop (step b) and increase the iteration number by $i = (i+1) \bmod N_F$.

Algorithm 1 Collision handling of two particles with positions $\vec{p_1}, \vec{p_2}$ and velocities $\vec{v_1}, \vec{v_2}$.

Require: diameter d, spring coefficient k, friction f_c, restitution e
  $\vec{p_{12}} \leftarrow \vec{p_2} - \vec{p_1}$
  $d_{12} \leftarrow |\vec{p_{12}}|$
  if $d_{12} < d$ **then**
    {Minimum translation distance}
    $\vec{m} \leftarrow \vec{p_{12}}\,((d - d_{12})/d_{12})$
    {Modify positions}
    $\vec{p_1} \leftarrow \vec{p_1} - \vec{m}/2$
    $\vec{p_2} \leftarrow \vec{p_2} + \vec{m}/2$
    {Impulse}
    $a \leftarrow \text{atan2}(\vec{p_{12}})$
    $\vec{i} \leftarrow d\,(\cos(a), \sin(a))$
    $\vec{i} \leftarrow k\,(\vec{i} - \vec{p_{12}})$
    {Modify velocities}
    $\vec{v_1} \leftarrow \vec{v_1} - \vec{i}$
    $\vec{v_2} \leftarrow \vec{v_2} + \vec{i}$
    {Reduce horizontal velocity based on angle a}
    $f_a \leftarrow f_c\,(1 - ((a + \pi/2)^2/(\pi/2)^2))$
    if $a < 0$ **then**
      $v_{1x} \leftarrow v_{1x}\,f_a\,(1 - e)$
    else
      $v_{2x} \leftarrow v_{2x}\,f_a\,(1 - e)$
    end if
  end if

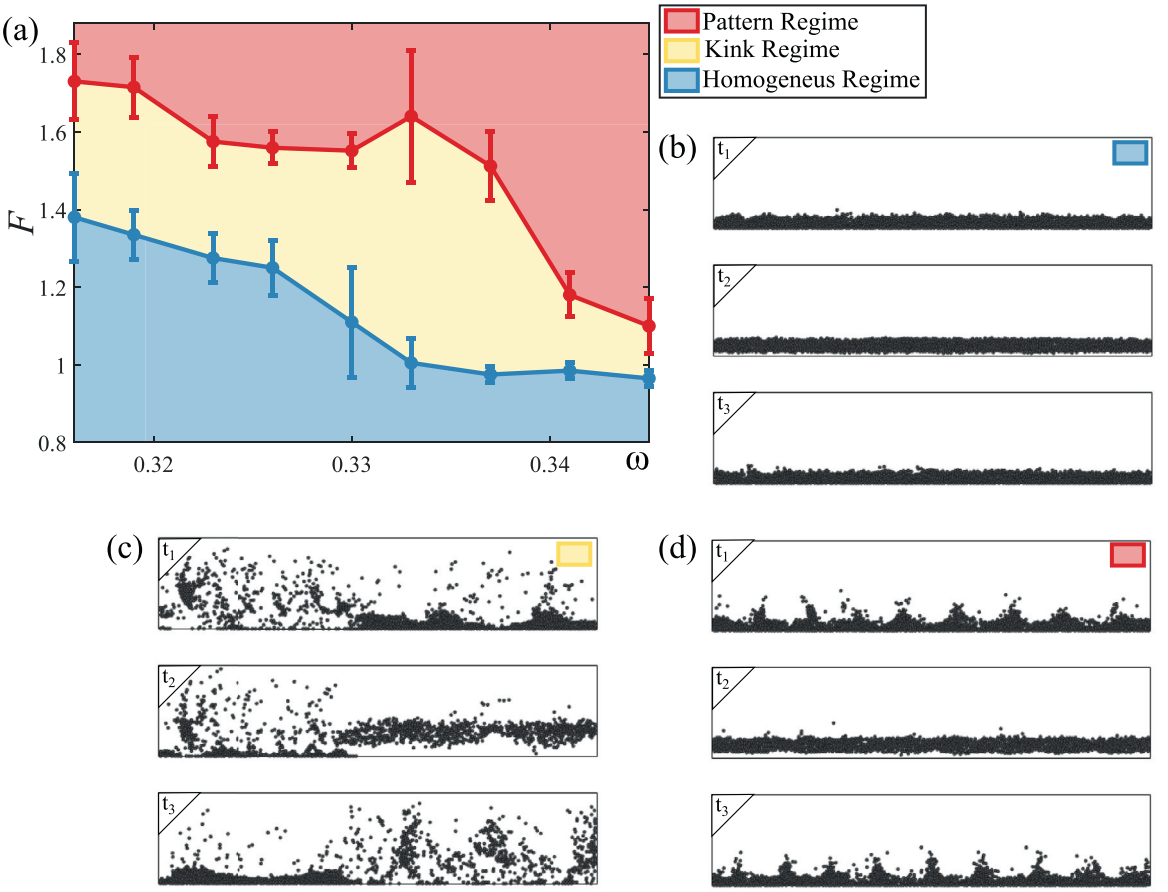

Fig. 3. Numerical analysis of particle-based model of quasi-two-dimensional shallow granular layer subjected to an airflow oscillating in time. (a) Numerical phase diagram for the pump force F versus the parameter ω. The error bars account for the standard deviation obtained in determining critical points. The light blue, yellow, and light red colors represents regions of the parameter space where, respectively, motionless granular layer, domains walls, and standing waves are observed. Temporal sequences of images for an oscillatory granular bed (b), granular domain (c), and standing wave (d) with $t_1 < t_2 < t_3$.

Since we use a time-step procedure (and not an event-driven algorithm), there is a possibility that particles overlap each other during the simulation. This case is handled in Algorithm 1, where additional friction is added to prevent the simulation from becoming unstable.

4. Numerical results

In numerical simulations, we have considered that h_m is greater than the motionless flat granular layer deposited at the bottom of the cell. For a very small strength of the pump force F, we observe that the granular layer remains motionless. Only few particles on the top of the surface of the granular medium are stirred. As the strength of the pumping increases, the granular layer fluidizes and oscillates with the frequency of forcing. Fig. 3(b) illustrates a temporal sequence of the typically observed images. As the frequency of the forcing cycle increases, we observe that the region where the oscillatory granular bed is observed decreases (cf. Fig 3), which is consistent with the experimental observations (see Fig. 1). At this stage the uniform granular bed is stable. However, increasing the intensity of the pumping to a critical value, we observe the appearance of domains that oscillate out of phase. The origin of this instability is of parametric nature [40]; monitoring the Fourier transform we observe the emergence of the mode with an $\omega/2$ frequency [38]. Experimentally, an analogous phenomenon is observed [15]. Namely, the parametric instability causes the emergence of domain walls or granular kinks in a quasi-two-dimensional shallow granular layer subjected to an air flow oscillating in time. Fig. 3(c) depicts a temporal sequence of the numerical granular kink. We observe that the maximum height difference between the domains decreases as one approaches the bifurcation point. Indeed, this parametric bifurcation is of the second-order type. It is important to mention that in the course of increasing the strength of the airflow, the domains exhibit a wavelength (cf. Fig. 3c). The yellow zone in Fig. 3 accounts for the region in the parameter space where we numerically observe the numerical granular kinks. This region has a tendency to slope with the frequency of forcing, in an analogous way to what was observed experimentally. By increasing the magnitude of the pump force even more, we observe that the granular domains become

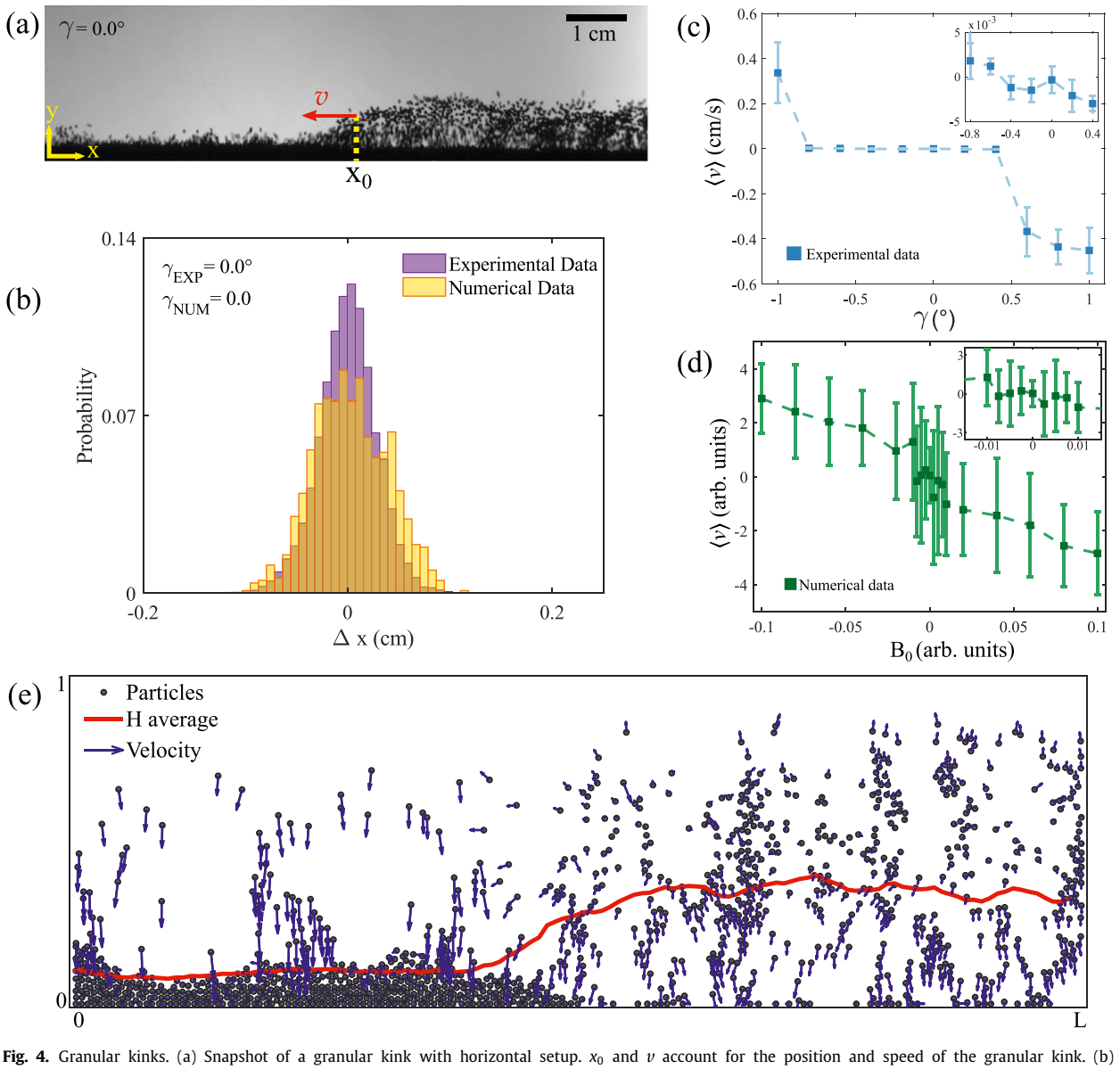

Fig. 4. Granular kinks. (a) Snapshot of a granular kink with horizontal setup. x_0 and v account for the position and speed of the granular kink. (b) Probability density distribution of granular kink displacements $\Delta x \equiv x_0(t_{i+1}) - x_0(t_i)$. Purple and yellow vertical rectangles account for the probability distribution obtained experimentally and numerically, respectively. (c) Experimental diagram of the average velocity $\langle v \rangle$ versus inclination angle γ of the experimental setup. Inset accounts for a magnification of the pinning region. (d) Numerical diagram of the average velocity $\langle v \rangle$ versus horizontal force B_0. Inset accounts for a magnification of the pinning region. (e) Numerical image of a granular kink. Gray discs represent the individual particles. The continuous red curve is the average height. The blue arrows show the velocity of particles. (For interpretation of the references to colour in this figure legend, the reader is referred to the web version of this article.)

unstable, and a standing wave emerges, with a well-defined wavelength, Faraday instability [31]. Fig. 3(d) shows a sequence of temporal images of the Faraday waves observed in the numerical simulations. The phase diagram found numerically is shown in Fig. 3a. This diagram is in excellent qualitative agreement with the one observed experimentally (see Fig. 1). The numerical bifurcation diagram was obtained by performing 20 numerical realizations for each point of the parameter space. The error bars shown in this figure account for the standard deviation obtained in determining critical points. Therefore, the proposed model adequately accounts for the self-organizing patterns observed experimentally.

4.1. Numerical granular kinks

One of the most intriguing dynamic phenomena are the granular kinks [11,15,16], (see Fig. 1b and Fig. 4). They correspond to particle-type states that are localized and described by continuous parameters such as their position [41,42]. The position of the granular kink x_0 is defined as the spatial location that corresponds to the average height between two

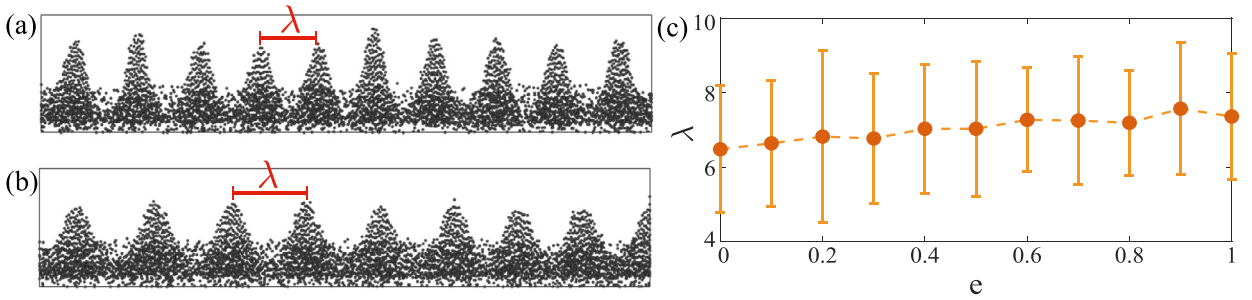

Fig. 5. Numerical Faraday waves. Profile of the fluidized granular layer for $e = 0$ (a) and $e = 1$ (b). (c) Wavelength λ as a function of the restitution coefficient e.

consecutive domains (cf. Fig. 4a). Recently, it has been shown experimentally that the displacement of the kink position, $\Delta x \equiv x_0(t_{i+1}) - x_0(t_i)$, satisfies a bell-shaped distribution [11]. The origin of this dynamical behavior is associated with the inherent fluctuations of the granular medium and the structure of the granular kink. Numerically, we have studied the evolution of the displacement distribution, and we have found a similar dynamical behavior to that observed experimentally. Fig. 4b shows the distribution and comparison of the displacement of the granular kink experimentally and numerically. As a function of the energy injection, strength, and period applied, we observe that the fluidized state may or may not be more dilute. The interface characterizes more diluted states exhibits greater fluctuations. For example, in the experimental snapshot and numerical simulation shown in Figs. 4a and 4 e, respectively, it is clearly observed that in the former, the granular bed is more diluted; that is, a higher energy injection is considered.

Another relevant phenomenon observed in granular kinks is the pinning-depinning transition [11]. This phenomenon is related to the fact that by tilting the experimental set-up in a range of small angles, the kink fluctuates erratically, and its average speed $\langle v \rangle$ is small (pinning region). However, starting from a critical value, granular kinks propagate in a more ballistic way (depinning region) that is, except for small random fluctuations, with a well-defined speed which increases proportionally to the angle. Fig. 4c shows the experimental pinning-depinning transition of a granular kink. To account for the tilt of the experimental setup, we have included the horizontal force B_0 when particles collide with the ground. In a range of small strength of B_0, we observe that the granular kinks have small average speeds (pinning region). However, from a critical strength B_0, granular kinks begin to propagate with remarkable speed (depinning region). This speed increases linearly with the intensity of the force (see Fig. 4d). Therefore, numerically we observe a pinning-depinning transition, similar to that observed experimentally.

An unsolved question is what is the internal granular structure of the granular kinks. As the experiment is not perfectly two-dimensional, this characterization is a thorny task since only particles in the foreground can characterize their position and speed. In the case of a vertically driven granular medium (oscillating container), experiments with perfectly two-dimensional granular media are possible [19]. In this type of experiment, the formation of convection rolls in the structure of granular kink has been established (heaping process). Our numerical simulations allow us to reveal the structure of granular kink by characterizing the position and velocity of the particles (see Fig. 4e). The domains have a periodic velocity structure, but the system does not exhibit roll formation [38]. Presumably, this is due to the presence of fluid passing through the granular bed (experimentally) and the force that pushes the particles into the bulk of the granular medium (experimentally and numerically). In experiments and numerical simulations with a vibrating container, where convection is observed, the force is only injected into the particles in contact with the container (external granular layers energy injection). Experimental work to verify this prediction is in progress.

4.2. Numerical faraday waves

As we have previously mentioned, for sufficient large strength of the forcing the system exhibits standing or Faraday waves, see Fig. 1. One of the unknown characteristics of these intriguing patterns is how they originate and what governs the length of the observed patterns. Usually, the wavelength is the competition of difference of scales of different transport processes, commonly denominated as Turing mechanism [43], or the stability exchange of spatial modes [44]. Fig. 5 summarizes how the wavelength changes with the restitution coefficient e. When increasing the restitution coefficient the wavelength increases. At first approximation, the wavelength is proportional to the coefficient of restitution. Physically, this phenomenon can be understood as a consequence of the fact that by increasing the coefficient of restitution, the particles can travel greater distances horizontally after a collision. As a matter of fact, changes in the transport mechanisms on the surface of the fluidized granular layer, allow the particles to be displaced at larger distances. Hence, the balance between the distances that the particles in the top granular layer can reach and the energy exchange fixes the wavelength of the Faraday waves.

5. Conclusions and remarks

Granular systems kept out of thermodynamic equilibrium by means of energy injection exhibit complex dynamic behaviors. A global understanding of these phenomena lacks a unified description due to the absence of fluid type theory. This is the principal difficulty in understanding and comparing them with molecular fluids. One strategy to achieve progress in this direction is to establish minimal models that describe well the dynamics and taking them as the point of departure, through coarse-graining processes, derive macroscopic models. The fundamental, intermediate step is to derive these minimal microscopic models and compare with experimental findings.

A natural strategy of describing granular media is by considering molecular dynamics due to their elemental constituents' simple interaction rules. In fluid-driven granular systems, this strategy should be complex since the dynamics at the microscopic level are described by particles and fluid equations. This methodology has successfully explained segregation, convection, fluidization, and the formation of sand ripples. However, given its complexity, this type of approach is not efficient to obtain a minimal microscopic model. Particle-based numerical simulations are one of the efficient strategies in this direction. Motivated by this idea, we have proposed here a minimal numerical model that captures the dynamics of a quasi-two-dimensional shallow granular layer subjected to an air flow oscillating in time. We have determined the phase diagram, the structure and dynamics of domain walls, the presence of the Faraday waves, and we have explained the origin of their wavelength. Our findings are in a very good qualitative agreement with experimental observations.

From this type of model, a kinetic theory can be established, within which the appropriate macroscopic physical quantities (mass density, granular height field, kinetic energy, and so forth) and the governing equations could be identified. Work in this direction is in progress.

Declaration of Competing Interest

The authors declare that they have no known competing financial interests or personal relationships that could have appeared to influence the work reported in this paper.

CRediT authorship contribution statement

B. Crespin: Software, Methodology, Formal analysis, Data curation, Visualization, Writing - review & editing. **M.G. Clerc:** Conceptualization, Validation, Resources, Investigation, Writing - original draft, Supervision, Project administration, Funding acquisition. **G. Jara-Schulz:** Investigation, Formal analysis, Data curation, Writing - review & editing, Visualization. **M. Kowalczyk:** Writing - review & editing, Validation, Conceptualization.

Acknowlgedgments

M.G.C. and G.J.S. and Millenium Institute for Research in Optics (MIRO), ANID–Millennium Science Initiative Program–ICN17_012. M.G.C. thanks for the financial support FONDECYT project 1180903. M. Kowalczyk was partially supported by Chilean research grants Fondecyt 1170164 and CMM Conicyt PIA AFB170001. B. Crespin was partially supported by a CNRS delegation grant.

Supplementary material

Supplementary material associated with this article can be found, in the online version, at doi:10.1016/j.cnsns.2021.105770.

References

[1] de Gennes PG. Granular matter: a tentative view. Rev Mod Phys 1999;71:S374.
[2] Duran J. Sands, powders, and grains: an introduction to the physics of granular materials. Springer Science & Business Media; 2012.
[3] Mehta A. Granular matter: an interdisciplinary approach. Springer Science & Business Media; 2012.
[4] Andreotti B, Forterre Y, Pouliquen O. Granular media: between fluid and solid. Cambridge University Press; 2013.
[5] Aranson I, Tsimring L. Granular patterns. Oxford University Press; 2009.
[6] Geldart D. Gas fluidization technology. New York: Wiley; 1986.
[7] Li J, Aranson IS, Kwok WK, Tsimring LS. Phys Rev Lett 2003;90:134301.
[8] Nicolis G, Prigogine I. Self-Organization in non equilibrium systems. New York: Wiley; 1977.
[9] Pismen LM. Patterns and interfaces in dissipative dynamics. Berlin: Springer; 2006.
[10] Walgraef D. Spatio-temporal pattern formation: with examples from physics, chemistry, and materials science. Springer Science & Business Media; 2012.
[11] Jara-Schulz G, Ferré MA, Falcón C, Clerc MG. Noise-induced kink propagation in shallow granular layers. Chaos, Solitons & Fractals 2020;134:109677.
[12] Li J, Aranson IS, Kwok WK, Tsimring LS. Periodic and disordered structures in a modulated gas-driven granular layer. Phys Rev Lett 2003;90:134301.
[13] Orellana CS, Aranson IS, Kwok WK, Rica S. Self-diffusion of particles in gas-driven granular layers with periodic flow modulation. Phys Rev E 2005;72:040301.
[14] Ortega I, Clerc MG, Falcón C, Mujica N. Subharmonic wave transition in a quasi-one-dimensional noisy fluidized shallow granular bed. Phys Rev E 2010;81:046208.
[15] Macías JE, Clerc MG, Falcón C, Garcia-Nustes MA. Spatially modulated kinks in shallow granular layers. Phys Rev E 2013;88:020201.
[16] Macías JE, Falcón C. Dynamics of spatially modulated kinks in shallow granular layers. New J Phys 2014;16:043032.

[17] Hui C, Wei-Zhong C, Guo-Qing M. Patterns in a two-dimensional annular granular layer. Chin Phys Lett 2013;30:044501.
[18] Clément E, Vanel L, Rajchenbach J, Duran J. Pattern formation in a vibrated two-dimensional granular layer. Phys Rev E 1996;53:2972.
[19] Peng Z, Guo-Qing M, Kai H, Yi Y, Rong-Jue W. Experimental observation of kink in a perfect bidimensional granular system. Chin Phys Lett 2005;22:1961.
[20] Herrmann HJ, Luding S. Modeling granular media on the computer. Continuum Mech Thermodyn 1998;10:189–231.
[21] Herrmann HJ. Simulation of granular media. Physica A 1992;191:263.
[22] Ramírez R, Risso D, Cordero P. Thermal convection in fluidized granular systems. Phys Rev Lett 2000;85:1230.
[23] Eshuis P, Van Der Weele K, Van Der Meer D, Bos R, Lohse D. Phase diagram of vertically shaken granular matter. Phys Fluids 2007;19:123301.
[24] Paolotti D, Barrat A, Marini Bettolo Marconi U, Puglisi A. Thermal convection in monodisperse and bidisperse granular gases: a simulation study. Phys Rev E 2004;69:1523.
[25] Pontuale G, Gnoli A, Reyes FV, Puglisi A. Thermal convection in granular gases with dissipative lateral walls. Phys Rev Lett 2016;117:098006.
[26] Luding S, Clément E, Rajchenbach J, Duran J. Simulations of pattern formation in vibrated granular media. EPL 1996;36:247.
[27] Argentina M, Clerc MG, Soto R. Van der waals-like transition in fluidized granular matter. Phys Rev Lett 2002;89:044301.
[28] Biswas P, Sanchez P, Swift MR, King PJ. Numerical simulations of air-driven granular separation. Phys Rev E 2003;68:050301.
[29] Tang Y, Lau YM, Deen NG, Peters EAJF, Kuipers JAM. Direct numerical simulations and experiments of a pseudo-2d gas-fluidized bed. Chem Eng Sci 2016;143:166.
[30] Durán O, Claudin P, Andreotti B. Direct numerical simulations of aeolian sand ripples. Proc Natl Acad Sci USA 2014;111:15665.
[31] Faraday M. On a peculiar class of acoustical figures; and on certain forms assumed by groups of particles upon vibrating elastic surfaces. Phil Trans R Soc (London) 1831;121:299–340.
[32] Agez G, Szwaj C, Louvergneaux E, Glorieux P. Noisy precursors in one-dimensional patterns. Phys Rev A 2002;66:063805.
[33] Luciani A, Habibi A, Manzotti E. A multi-scale physical model of granular materials. In Graphics interface 1995;95:136–46.
[34] Bell N, Yu Y, Mucha PJ. Particle-based simulation of granular materials. In ACM SIGGRAPH/Eurographics Symposium on Computer Animation 2005:77–86.
[35] Martelloni G, Bagnoli F, Guarino A. A 3D model for rain-induced landslides based on molecular dynamics with fractal and fractional water diffusion. Cambridge University Press; 2009. Communications in Nonlinear Science and Numerical Simulation; 50, 2017
[36] Green S. Particle simulation using cuda. In CUDA Toolkit documentation, NVIDIA Corporation 2010.
[37] Zhao Z, Zhang J, Z G. Numerical simulation of sand flow using molecular dynamics approach. In: Proceedings of GeoShanghai 2018 In- ternational Conference: Fundamentals of Soil Behaviours Springer Singapore; 2018.
[38] See the video in the supplementary material.
[39] Garay J, Ortega I, Clerc MG, Falcón C. Symmetry-induced pinning-depinning transition of a subharmonic wave pattern. Phys Rev E 2012;85:035201.
[40] Landau LD, Lifshiftz EM. Mechanics, vol. 1 course of theoretical physics. Pergamon Press; 1976.
[41] Manton N, Sutcliffe P. Topological solitons. Cambridge University Press; 2004.
[42] Vachaspati T. Kinks and domain walls: an introduction to classical and quantum solitons. Cambridge University Press; 2006.
[43] Turing A. The chemical basis of morphogenesis. Phil Trans R Soc B 1952;237:37.
[44] Cross M, Greenside H. Pattern formation and dynamics in nonequilibrium systems. Cambridge University Press; 2009.